Dithiazolodithiazolyl Radicals: Substituent Effects on Solid State Structures and Properties

Leanne Beer,[†] James F. Britten,[‡] Owen P. Clements,[†] Robert C. Haddon,[§] Mikhail E. Itkis,[§] Kristin M. Matkovich,[†] Richard T. Oakley,*[,†] and Robert W. Reed[†]

Department of Chemistry, University of Waterloo, Waterloo, Ontario N2L 3G1, Canada, Department of Chemistry, McMaster University, Hamilton, Ontario L8S 4M1, Canada, and Department of Chemistry and Center for Nanoscale Science and Engineering, University of California, Riverside, California 92521-0403

Received November 18, 2003. Revised Manuscript Received February 13, 2004

A general synthetic route to the pyridine-bridged dithiazolodithiazolyl framework R_2BPR_1, involving N-alkylation of a 4-substituted 2,6-dichloropyridine, followed by amination and double Herz cyclization with S_2Cl_2, has been developed. The radicals R_2BPMe (R_2 = Me, Ph) have been prepared and characterized by EPR spectroscopy and cyclic voltammetry. Their crystal structures have been determined by X-ray crystallography. Both structures consist of undimerized slipped radical π-stacks. Lateral interactions in MeBPMe (space group $P2_1/c$) generate chainlike arrays with radicals linked by inversion centers; there are no close interchain S−S contacts. By contrast, in PhBPMe (space group $P3_121$) the radical π-stacks are nested about 3_1 axes, so as to produce an extensive 2-dimensional network of intermolecular S−S interactions. Variable-temperature magnetic susceptibility measurements reveal that MeBPMe is essentially paramagnetic, whereas PhBPMe displays strong antiferromagnetic coupling. A value of $J = -149$ cm^{-1} has been estimated by using a Bonner−Fisher anti-ferromagnetic chain model. Pressed pellet conductivity measurements indicate values of $\sigma_{RT} \approx 10^{-5}$ S cm^{-1} for both R_2BPMe compounds (R_2 = Me, Ph), suggesting Mott insulator ground states. The structural results and transport properties are discussed in the light of extended Hückel theory band structure calculations.

Introduction

The concept of using neutral radicals as building blocks for molecular conductors provides an appealing alternative to conventional charge-transfer salts.[1] The model is based on the idea that a stacked array of π-radicals, each with one unpaired electron, will be associated with a half-filled energy band, and hence possess a metallic ground state.[2] There are, however, several shortcomings to this model. First, any 1-dimensional half-filled energy band is prone to Peierls instability, i.e., the radicals associate into closed shell dimers.[3] Second, if dimerization can be suppressed, e.g., by steric bulk, the resulting low bandwidth W, coupled with the high on-site Coulomb repulsion energy U associated with a half-filled band, leads to a Mott insulating state.[4] Essentially the spins are trapped on the radicals and charge transport is suppressed. Improved conductivity thus requires materials with a high W/U ratio, i.e., systems with a large bandwidth and a small on-site Coulomb repulsion energy.

For some time we have pursued the design of radical conductors using inorganic radicals based on heterocyclic thiazyl/selenazyl frameworks.[5] Although the a priori estimation of the magnitude of both W and U for these systems is not practical, trends in the gas-phase disproportionation enthalpy ΔH_{disp}[6] for a series of related radicals provide a working mirror to the trends in U. Gas-phase ionization potentials (IP) can be obtained experimentally,[7] but reliable estimates of both IP and electron affinity (EA) values can be easily obtained by

* To whom correspondence should be addressed. E-mail: oakley@sciborg.uwaterloo.ca.
[†] University of Waterloo.
[‡] McMaster University.
[§] University of California, Riverside.

(1) (a) Marsitzky, D.; Mullen, K. In *Advances in Synthetic Metals*; Bernier, P., Lefrant, S., Bidan, G., Eds.; Elsevier: 1999; p 1. (b) Grossel, M. C.; Weston, S. C. *Contemp. Org. Synth.* **1994**, *1*, 317. (c) Williams, J. M.; Ferraro, J. R.; Thorn, R. J.; Carlson, K. D.; Geiser, U.; Wang, H. U.; Kini, A. M.; Whangbo, M.-H. *Organic Superconductors (Including Fullerenes)*; Prentice Hall: Englewood Cliffs, NJ, 1992. (d) Ferraro, J. R.; Williams, J. M. *Introduction to Synthetic Electrical Conductors*; Academic Press: New York, 1987; p 25.

(2) (a) Haddon, R. C. *Nature* **1975**, *256*, 394. (b) Haddon, R. C. *Aust. J. Chem.* **1975**, *28*, 2333. (c) Haddon, R. C. *Aust. J. Chem.* **1975**, *28*, 2334.

(3) Peierls, R. C. *Quantum Theory of Solids*; Oxford University Press: London, 1953; p 108.

(4) Mott, N. F. *Metal−Insulator Transitions*; Taylor and Francis: London, 1990.

(5) For recent examples, see (a) Beer, L.; Cordes, A. W.; Myles, D. J. T.; Oakley, R. T.; Taylor, N. J. *CrystEngComm* **2000**, 20. (b) Britten, J. F.; Clements, O. P.; Cordes, A. W.; Haddon, R. C.; Oakley, R. T.; Richardson, J. F. *Inorg. Chem.* **2001**, *40*, 6820. (c) Cordes, A. W.; Haddon, R. C.; Oakley, R. T. *Adv. Mater.* **1994**, *6*, 798. (d) Cordes, A. W.; Haddon, R. C.; Oakley, R. T. In *The Chemistry of Inorganic Ring Systems*; Steudel, R., Ed.; Elsevier: Amsterdam, 1992; p 295.

(6) ΔH_{disp} is the enthalpy change for the conversion of two gas-phase radicals R into a cation/anion pair, i.e., $2\,R \rightleftarrows R^+ + R^-$, and accordingly is equal to the difference between the ionization potential (IP) and electron affinity (EA). The solution-based cell potential $E_{cell} = E_{1/2}(ox) - E_{1/2}(red)$ is the difference between the half-wave potentials for the oxidation and reduction processes.

10.1021/cm035191u CCC: $27.50
Published on Web 03/26/2004

Chart 1

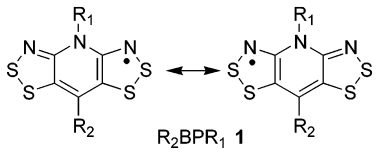

computation.[8,9] Alternatively, solution based cell potentials E_{cell}, which are generally accessible by experiment, provide an effective mirror to solid-state characteristics.[10] Using either criterion, the working prescription for good conductivity requires radicals with good ion energetics, i.e., low ΔH_{disp} and E_{cell} values. The resonance-stabilized 1,2,3-dithiazolo-1,2,3-dithiazolyl (or bis-DTA) framework R_2BPR_1 **1** represents an appealing system, conforming to both the energetic and structural criteria noted above. Recently, we reported the synthesis and structural characterization of the first examples (R_1 = Me, Et, Pr; R_2 = Cl; R_1 = Me, Et; R_2 = H) of this class of radical.[11,12] These radicals are exceptionally soft,[13] i.e., have low ΔH_{disp} values, and in the solid state display a rich network of intermolecular S−S interactions, which collectively give rise to significant electronic bandwidth *W*. Despite these favorable features, however, Mott insulating behavior prevails, with room-temperature conductivities $\sigma RT \approx 10^{-5}$ S cm^{-1}.

Whereas the value of *U* in bis-DTAs is unlikely to change as a function of R_1 and R_2, the electronic bandwidth *W* will very much depend on the way in which the substituents modify solid-state packing. To explore these issues we have sought to develop synthetic routes to R_2BPR_1 **1** radicals, with the focus being on the need to incorporate a wide range of substituents in the R_2 site. Herein we describe the preparation, EPR, and electrochemical characterization of the methyl- and phenyl-substituted compounds MeBPMe and PhBPMe **1** (R_1 = Me; R_2 = Me, Ph). We also report their crystal structures, magnetic, and conductivity properties, and interpret the results in the light of extended Hückel theory (EHT) band calculations.

Results

Synthesis. We have reported a convenient synthesis of bis-DTA derivatives by using a "double Herz" condensation of *N*-methyl-2,6-diaminopyridinium triflate **2** (R_2 = H) with sulfur monochloride (Scheme 1).[11] If the reaction is performed at reflux in acetonitrile, the product is the triflate salt of the corresponding chloro-substituted cation, i.e., [**1**][OTf] (R_1 = Me, R_2 = Cl). Using milder reaction conditions (room temperature in the presence of an auxiliary base) the prototypal derivatives [**1**][Cl] (R_1 = Me, R_2 = H) can be obtained.[12]

Scheme 1

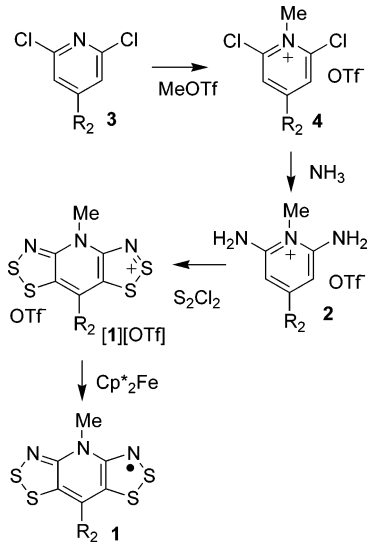

To explore the generality of this reaction, with a view to incorporating a range of R_2 substituents into the bis-DTA framework, we have developed a straightforward method for preparing 4-substituted 2,6-diaminopyridinium salts [**2**][OTf] (R_2 = H, Me, Ph) starting from the corresponding 2,6-dichloropyridine **3**. Thus, methylation of **3** (R_2 = H, Me, Ph) with methyl triflate provides the *N*-methylated salt **4** (R_2 = H, Me, Ph) in high yield. Treatment of **4** with ammonia[14] in acetonitrile then affords the desired *N*-methyl-diaminopyridinium triflate **2** (R_2 = H, Me, Ph). The double Herz condensation of **2** (R_2 = Me, Ph) with S_2Cl_2 at reflux in acetonitrile proceeds in moderate to high yields to give the appropriate bis-DTA triflate [**1**][OTf] (R_1 = Me; R_2 = Me, Ph), although for R_2 = Me reaction times must be minimized in order to prevent chlorination of the methyl group. As in our earlier work, decamethylferrocene serves as an effective one-electron reducing agent for converting the salts [**1**][OTf] (R_1 = Me; R_2 = Me, Ph) into the radicals **1**, i.e., MeBPMe and PhBPMe.

EPR Spectra and Electrochemistry. The X-band EPR spectra of R_2BPMe (R_2 = Me, Ph), recorded in CH_2Cl_2 at room temperature, are similar to those observed for other bis-DTA radicals, with a rich hyperfine pattern dominated by coupling to two equivalent dithiazolyl nitrogens, the value of a_N being approximately one-half of that observed in monofunctional 1,2,3-DTA radicals.[15] There is also weaker coupling to the pyridine nitrogen and to the *N*-methyl protons. The presence of a phenyl group in PhBPMe introduces additional coupling, as a result of which the spectrum collapses to a broad

(7) (a) Boeré, R. T.; Oakley, R. T.; Reed, R. W.; Westwood, N. P. C. *J. Am. Chem. Soc.* **1989**, *111*, 1180. (b) Cordes, A. W.; Goddard, J. D.; Oakley, R. T.; Westwood, N. P. C. *J. Am. Chem. Soc.* **1989**, *111*, 6147. (c) Cordes, A. W.; Bryan, C. D.; Davis, W. M.; de Laat, R. H.; Glarum, S. H.; Goddard, J. D.; Haddon, R. C.; Hicks, R. G.; Kennepohl, D. K.; Oakley, R. T.; Scott, S. R.; Westwood, N. P. C. *J. Am. Chem. Soc.* **1993**, *115*, 7232. (d) Brownridge, S.; Du, H.; Fairhurst, S. A.; Haddon, R. C.; Oberhammer, H.; Parsons, S.; Passmore, J.; Schriver, M. J.; Sutcliffe, L. H.; Westwood, N. P. C. *J. Chem. Soc., Dalton Trans.* **2000**, 3365.

(8) Kaszynski, P. *J. Phys. Chem. A* **2001**, *105*, 7626.

(9) Cordes, A. W.; Mingie, J. R.; Oakley, R. T.; Reed, R. W.; Zhang, H. *Can. J. Chem.* **2001**, *79*, 1352.

(10) Boeré, R. T.; Roemmele, T. L. *Coord. Chem. Rev.* **2000**, *210*, 369.

(11) Beer, L.; Brusso, J. L.; Cordes, A. W.; Haddon, R. C.; Itkis, M. E.; Kirschbaum, K.; MacGregor, D. S.; Oakley, R. T.; Pinkerton, A. A.; Reed, R. W. *J. Am. Chem. Soc.* **2002**, *124*, 9498.

(12) Beer, L.; Britten, J. F.; Brusso, J. L.; Cordes, A. W.; Haddon, R. C.; Itkis, M. E.; MacGregor, D. S.; Oakley, R. T.; Reed, R. W.; Robertson, C. M. *J. Am. Chem. Soc.* **2003**, *125* (47), 14394−14403.

(13) (a) Pearson, R. G. *Struct. Bonding (Berlin)* **1993**, *80*, 2. (b) Pearson, R. G. *J. Chem Educ.* **1988**, *64*, 561.

(14) Rokach, J.; Hamel, P.; Hunter, N. R.; Reader, G.; Rooney, C. S.; Anderson, P. S.; Cragoe, E. J., Jr.; Mandel, L. R. *J. Med. Chem.* **1979**, *22*, 237.

(15) (a) Cordes, A. W.; Mingie, J. R.; Oakley, R. T., Reed, R. W.; Zhang, H. *Can. J. Chem.* **2001**, *79*, 1352. (b) Barclay, T. M.; Beer, L.; Cordes, A. W.; Oakley, R. T.; Preuss, K. E.; Taylor, N. J.; Reed, R. W. *Chem. Commun.* **1999**, 531. (c) Preston, K. F.; Sutcliffe, L. H. *Magn. Reson. Chem.* **1990**, *28*, 189.

Table 1. EPR Hyperfine Coupling Constants (mT) and *g*-Values of R_2BPMe

	ClBPMe	HBPMe	MeBPMe	PhBPMe
N(S) a_N	0.310 (2N)	0.313 (2N)	0.317 (2N)	0.32 (2N)
N(Me) a_N	0.060 (1N)	0.062 (1N)	0.060 (1N)	*a*
Me a_H	0.030 (3H)	0.034 (3H)	0.033 (3H)	*a*
R_2 a_R	0.030/0.024 (1Cl)	0.230 (1H)	0.227 (3H)	
g-value	2.0083	2.0082	2.0084	2.0086

[a] Coupling unresolved.

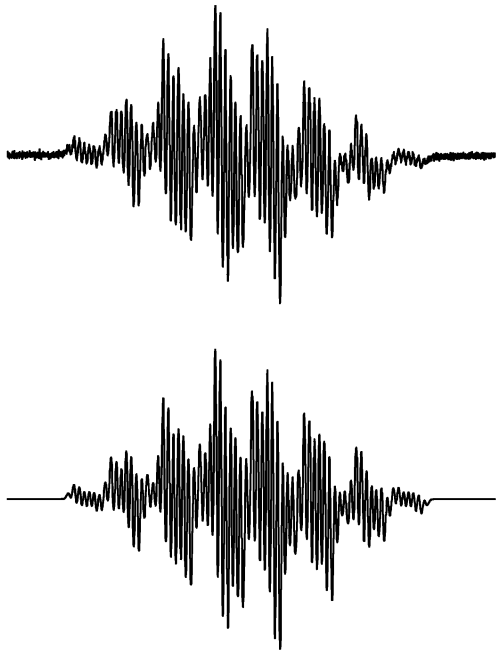

Figure 1. EPR spectrum of MeBPMe in CH_2Cl_2 (above) and simulation (below); SW = 3.0 mT; *L*/*G* ratio = 1.00; LW = 0.01 mT.

Table 2. Solution Half-Wave[a] and Cell[b] Potentials (V) for R_2BPMe Radicals 1 (R_2 = Cl, H, Me, Ph)

	$E_{1/2}(^{-1}/_0)$	$E_{1/2}(^0/_{+1})$	$E_{1/2}(^{+1}/_{+2})$	E_{cell}
ClBPMe	−0.835	0.005	1.415	0.830
HBPMe	−0.95[c]	−0.130	1.294	0.78[d]
PhBPMe	−0.956	−0.104	1.305	0.852
MeBPMe	−0.94[c]	−0.136	1.278	0.86[d]

[a] In CH_3CN, ref. SCE. [b] $E_{cell} = E_{1/2}(^0/_{+1}) - E_{1/2}(^{-1}/_0)$. [c] Irreversible behavior, E_{pc} value quoted. [d] E_{cell} estimated as $E_{pc}(^0/_{+1}) - E_{pc}(^{-1}/_0)$.

unresolved quintet, from which only the largest a_N coupling constant can be extracted (Table 1). For MeBPMe, however, a well resolved spectrum is observed (Figure 1), and all the *a* values, including those from the basal (R_2) methyl group, were extracted by full spectral simulation.

The results of cyclic voltammetric (CV) measurements on the [R_2BPMe][OTf] salts (R_2 = Me, Ph) are summarized in Table 2. As with other bis-DTA derivatives three waves are observed (Figure 2), corresponding to the $^{-1}/_0$, $^0/_{+1}$, and $^{+1}/_{+2}$ processes. In the case of PhBPMe all three waves are reversible, as they are in ClBPMe. For MeBPMe however, the $^{-1}/_0$ process is irreversible (as it is for HBPMe). This feature we attribute to the more electropositive core of these latter radicals, and a greater tendency toward cleavage of one of the S−S[16] (or S−N)[17] bonds upon reduction of the radical. The effect of the more electropositive core is also manifested in the $E_{1/2}$ values, which are shifted by 100−150 mV to more anodic potentials relative to those seen in ClBPMe. Nonetheless, the trends in both $E_{1/2}$ and E_{cell} map well onto those observed for ClBPR radicals, and are broadly consistent with the computed gas phase IP, EA, and disproportionation enthalpy (ΔH_{disp} = IP − EA) data for a model HBPH radical.[11]

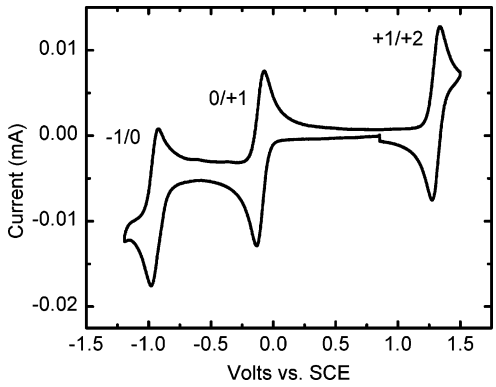

Figure 2. CV scan of [PhBPMe][OTf] in CH_3CN, [*n*-Bu_4N]-[PF_6] supporting electrolyte.

Table 3. Crystallographic Data

	MeBPMe	PhBPMe
formula	$C_7H_6N_3S_4$	$C_{12}H_8N_3S_4$
fw	260.39	322.45
a, Å	3.9919(7)	16.182(3)
b, Å	17.836(3)	16.182(3)
c, Å	13.888(2)	4.2947(12)
α, deg	90.0	90.0
β, deg	95.901(7)	90.0
γ, deg	90.0	120.0
V, Å^3	983.5(3)	974.0(4)
ρ(calcd), g cm^{-3}	1.758	1.649
space group	$P2_1/c$	$P3_121$
Z	4	3
temp, K	295(2)	295(2)
μ, mm^{-1}	8.554	0.718
λ, Å	1.54178	0.71073
data/restraints/parameters	2674/0/128	1500/0/101
solution method	direct methods	direct methods
R, *Rw* (on F^2)[a]	0.0685, 0.1549	0.0363, 0.0725

[a] $R = [\sum||F_o| - |F_c||]/[\sum|F_o|]$ for $I > 2\,\sigma(I)$; $R_w = \{[\sum w||F_o|^2 - |F_c|^2|^2]/[\sum(w|F_o|^4)]\}^{1/2}$.

Crystal Structures. Crystal data for R_2BPMe **1** (R_1 = Me; R_2 = Me, Ph) are summarized in Table 3, and a summary of pertinent intra- and intermolecular distance and angle information is given in Table 4. From a molecular perspective the bond lengths in each compound are slightly shorter than those seen in, for example, the oxidized ring of [**1**][SbF_6] (R_1 = H, R_2 = Cl).[18] Occupation of the antibonding SOMO[11] of the radical leads to a general elongation of the S−S, S−N, and S−C bonds, but the changes are smaller than those seen between monofunctional DTA radicals and their cations,[19] where the SOMO is localized on a single DTA

(16) Antonello, S.; Benassi, R.; Gavioli, G.; Taddei, F.; Maran, F. *J. Am. Chem. Soc.* **2002**, *124*, 7529.

(17) Alternatively, N−S bond cleavage could occur. See for example, Barclay, T. M.; Cordes, A. W.; Goddard, J. D.; Mawhinney, R. C.; Oakley, R. T.; Preuss, K. E.; Reed, R. W. *J. Am. Chem. Soc.* **1997**, *119*, 12136.

(18) Cordes, A. W.; Haddon, R. C.; Oakley, R. T.; Schneemeyer, L. F.; Waszczak, J. V.; Young, K. M.; Zimmerman, N. M. *J. Am. Chem. Soc.* **1991**, *113*, 582.

(19) (a) Barclay, T. M.; Beer, L.; Cordes, A. W.; Oakley, R. T.; Preuss, K. E.; Taylor, N. J.; Reed, R. W. *Chem. Commun.* **1999**, 531. (b) Beer, L.; Cordes, A. W.; Haddon, R. C.; Itkis, M. E.; Oakley, R. T.; Reed, R. W.; Robertson, C. M. *Chem. Commun.* **2002**, 1872.

Table 4. Summary of Intra- and Intermolecular Structural Parameters

	MeBPMe	PhBPMe
Intramolecular Distances (Å)[a]		
S−S	2.093(13)	2.0994(12)
S−N	1.666(16)	1.659(3)
Intermolecular Contacts (Å)[b] and Angles (°)		
d1	3.368(2)	3.287(1)
d2		3.507(1)
d3		3.467(1)

[a] Bond lengths cited are average values; numbers in parentheses are the larger of the ESD or the range. [b] See Figures 3, 6, and 7 for definitions of d1−d3.

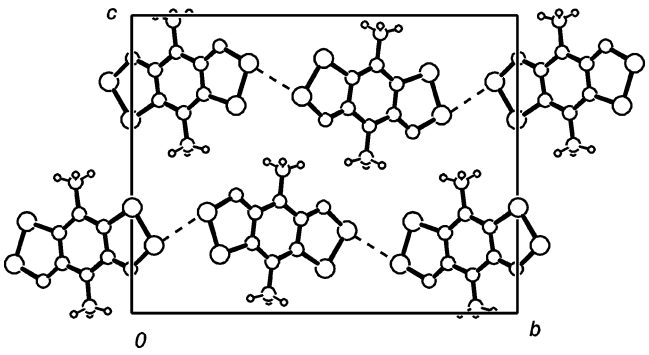

Figure 3. Unit cell of MeBPMe, viewed along the *x* direction. The S1−S1′ contact d1 is shown with dashed lines.

ring, and comparable to those seen between closed-shell benzo-bis(dithiazoles) and their radical cations.[20]

Crystals of MeBPMe belong to the monoclinic space group $P2_1/c$, and consist of π-stacked arrays of undimerized radicals running along the *x* direction. The molecules are planar to within 0.037 Å. Figure 3 shows the unit cell, as viewed down the stacking axis, and illustrates the chainlike arrangement of radicals running parallel to *y*. Linking these chains is a single intermolecular S1−S1′ interaction (d1 = 3.368(2) Å) which is inside the van der Waals contact for two sulfurs (3.6 Å).[21] There are no S−S contacts between the chains; the methyl groups on either side of the molecules serve as buffers to keep neighboring chains apart. Figure 4A shows a cartoon representation of this packing along with an analogous drawing of the arrangement of the radicals in R_2BPMe **1** (R_2 = H, Cl), which display a more zigzag chain motif (Figure 4B) with radicals along the chain being twisted so as to allow close head-to-head S−S contacts between, as well as along, the chains. In HBPMe these contacts cluster about inversion centers, whereas in ClBPMe they are related by 2_1 axes. The preference for straight or buckled chains can be traced back to the relative sizes of the belt-line R_1 and R_2 groups. Thus, in MeBPMe, the two sides (defined in terms of R_1 and R_2) of the molecule are almost identical, and close nesting of essentially linear chains is possible. When the two sides are more disparate, however, the zigzag motif is found, with the two R_1 and two R_2 groups occupying the resulting intermolecular cavity. The electronic consequences of the absence of interchain S−S interactions in MeBPMe are discussed below.

(20) (a) Barclay, T. M.; Cordes, A. W.; Oakley, R. T.; Preuss, K. E.; Reed, R. W. *Chem. Mater.* **1999**, *11*, 164. (b) Barclay, T. M.; Cordes, A. W.; Mingie, J. R.; Oakley, R. T.; Preuss, K. E. *CrystEngChem* **2000**, 15.

(21) Bondi, A. *J. Phys. Chem.* **1964**, *68*, 441.

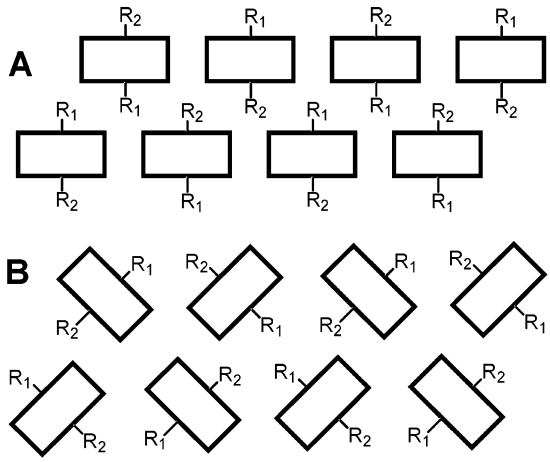

Figure 4. Orientations of radical chains in R_2BPR_1 **1**, (R_1 = Me): **A** (R_2 = Me), and **B** (R_2 = H, Cl).

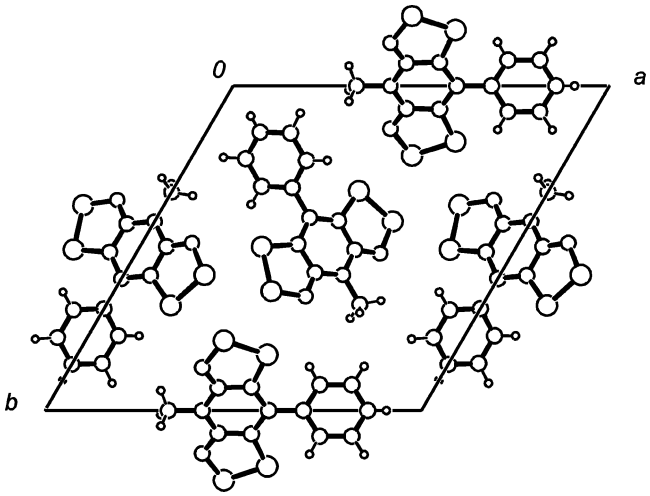

Figure 5. Unit cell of PhBPMe viewed along the *z* direction.

Like MeBPMe, the crystal structure of PhBPMe consists of slipped π-stacks running along the z direction. In contrast to MeBPMe, there is a slight ruffling of the molecules, as a result of which the S1 and N1 atoms are tipped out of the mean plane (by 0.197 and 0.120 Å, respectively). A view of the unit cell down the stacking axis is shown in Figure 5. As can be seen the radicals form intersecting chains running parallel to both *x* and *y*. The chains adopt a zigzag orientation as found in the R_2BPMe (R_2 = H, Cl) structures. However, as a result of the large size of the phenyl groups and the pseudo triangular shape of the molecule, the trigonal space group $P3_121$ is adopted, and, given this crystal symmetry, the arrangement of radicals in the *xy* plane resembles a set of close-packed "wheels" (Figure 6), with the methyl and phenyl groups being corralled within these wheels. At the connector points for the wheels, the radicals are related by 3_1 screw axes, to produce a strong network of lateral S−S interactions. Figure 7 illustrates one of these 3-fold spiral arrays, as viewed from the side, and defines the close contacts between the inner (S1) and outer (S2) atoms along the spiral. Of these, the S1−S1′ contact d1 (3.287(1) Å) along the spiral backbone is, to our knowledge, the shortest ever observed in a formally undimerized thiazyl radical. In addition, each S1 atom is linked by slightly longer

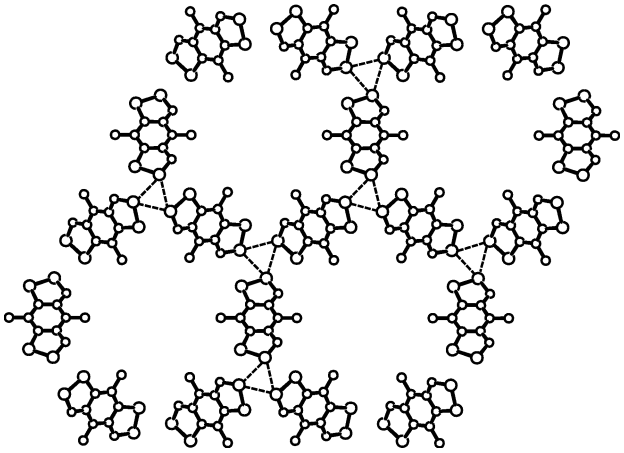

Figure 6. Close-packed "wheels" of PhBPMe radicals (phenyl groups omitted for clarity). Dashed lines indicate close S1−S1′ interactions (d1) about 3_1 axes.

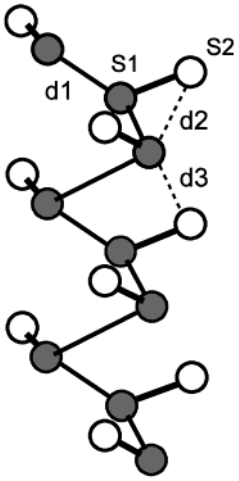

Figure 7. Spirals of S−S contacts about 3_1 axes in PhBPMe. Internal S1 atoms are shaded.

interactions d2 (3.507(1) Å) and d3 (3.467(1) Å) to neighboring S2′ atoms.

In both MeBPMe and PhBPMe the radicals form slipped π-stacks which pack into corrugated or herringbone arrays, as illustrated in Figure 8. The slipped stacks themselves can be characterized in terms of the slippage angle τ and the perpendicular separation δ between the mean planes (Figure 9). A comparison of the observed values for τ and δ in the known R_2BPMe **1** radicals (Table 5) reveals a fairly tight distribution over a range of τ values known[12] to be associated with somewhat weak intermolecular overlap along the stacks. These issues, and their effect on conduction bandwidths, are explored below.

Magnetic and Conductivity Measurements. Magnetic susceptibility (χ) measurements on MeBPMe reveal a temperature dependence (Figure 10A) which is consistent with normal Curie−Weiss[22] behavior for a $S = {}^1/_2$ system. Values of χ_0, C, and Θ are provided in Table 6. A plot of χT against T (Figure 10C) is relatively constant over the range 50−300 K, although the value of χT is a little less than that expected (0.375) for a $S = {}^1/_2$ system. Below 50 K a slight antiferromagnetic tail

(22) Carlin, R. L. *Magnetochemistry*; Springer-Verlag: New York, 1986.

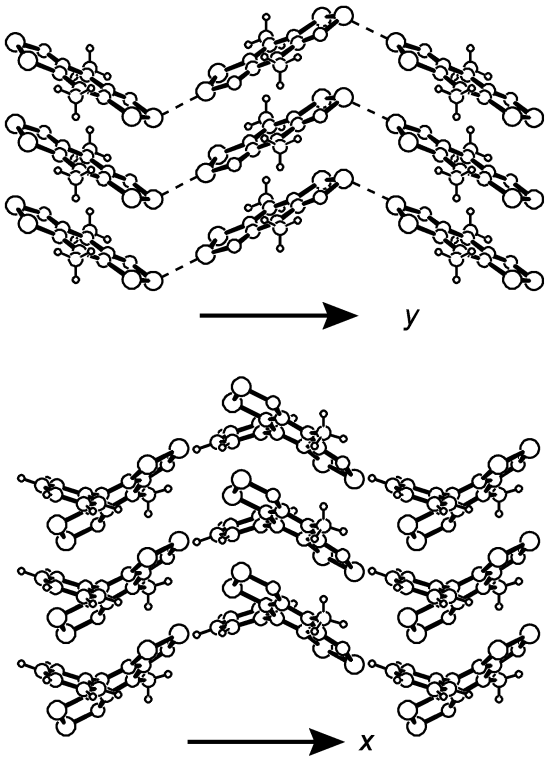

Figure 8. Herringbone arrays of radical π-stacks in MeBPMe (above) and PhBPMe (below).

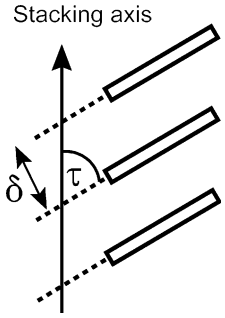

Figure 9. Definition of slippage angle τ and interplanar separation δ.

Table 5. π−Stack Slippage and Interplanar Separation Parameters in R_2BPMe Radicals

	HBPMe[b]	ClBPMe[c]	MeBPMe	PhBPMe
τ[a] (deg)	62.04(7)	54.81(13)	61.34(2)	55.92(16)
δ[a] (Å)	3.598(8)	3.470(5)	3.53(5)	3.557(6)

[a] See Figure 9 for definitions of τ and δ. [b] Reference 13. [c] Reference 12.

is observed. These properties mirror those found in HBPMe and ClBPMe, although in the latter two cases weak ferromagnetic coupling was observed at lower temperatures. In contrast to all of these systems, a plot of χ vs T for PhBPMe (Figure 10B) shows a marked deviation from Curie Weiss behavior, with the value of χ rising to a maximum and then falling away with decrease in T. The values of χ_0, C, and Θ extracted from a Curie−Weiss fit to the data above 230 K (Table 6) indicate a strongly antiferromagnetically coupled system. The rapid decrease in a plot of χT vs T (Figure 10C) below 300 K also heralds strong antiferromagnetic coupling. By applying a Bonner−Fisher anti-ferromag-

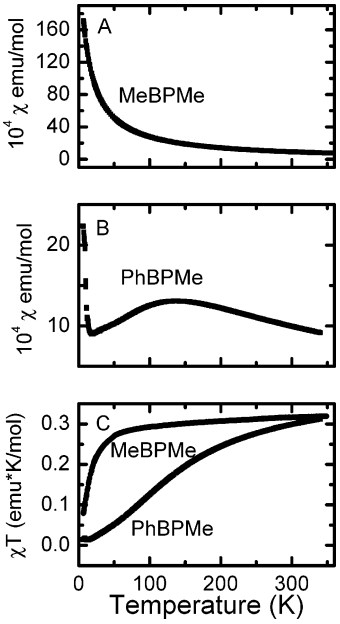

Figure 10. Plots of χ (A and B) and $\chi T(C)$ as a function of T for R_2BPMe **1** (R_2 = Me, Ph).

Table 6. Magnetic Data for R_2BPMe Radicals

compound	χ_0 (emu mol^{-1})	C	Θ (K)
MeBPMe[a]	−126 H 10^{-6}	0.326	−12
PhBPMe[b]	−172 H 10^{-6}	0.475	−177

[a] From a fit to the data above 5 K. [b] From a fit to the data above 230 K.

netic chain model,[23] we can estimate the value of J by setting $k\mathrm{T}_{max}/|J| = 0.641$, where T_{max} (= 137 K) is defined by the maximum value of χ in Figure 10B. Using this approximation we derive a value of $J = -149$ cm^{-1} (or 213 K). This value is large in comparison to those seen in other radical π-stacks,[24] but somewhat smaller than that found ($J = -465$ cm^{-1}) for the π-stacked dimer radical ion array in $[(S_2N_2C)C_6H_4(CN_2S_2)]_2[Cl]_3$.[25]

Pressed-pellet conductivity measurements on R_2-BPMe **1** (R_2 = Me, Ph) reveal room-temperature conductivities in the order of 10^{-5} S cm^{-1}, i.e., in the same range as those found for the R_2BPMe **1** (R_2 = Cl, H) series, indicative of Mott insulating behavior.

Band Calculations. To place the structural, magnetic, and conductivity results in context, we have probed the solid-state band structures of the pair of R_2-BPMe (R_2 = Me, Ph) radicals by extended Hückel theory (EHT) methods. The results must be viewed with caution, as the approach cannot be expected to succeed in systems where the tight-binding approximation fails, e.g., in Mott insulators. Figure 11 shows EHT dispersion curves, plotted along the stacking direction,[26] for the crystal orbitals arising from the SOMOs of the unit cell. These curves, four for MeBPMe ($Z = 4$) and three for PhBPMe ($Z = 3$) would constitute the half-filled conduction band if the materials were metallic. The magnetic and conductivity data, however, indicate Mott insulating states, in which each orbital within the bands is half-filled.[27] Regardless of the manner of band filling, however, the dispersion curves provide insight into the extent of the intermolecular interactions along and perpendicular to the slipped π-stacks, and provide qualitative estimates of the bandwidth W that can be compared with those found for other structures.

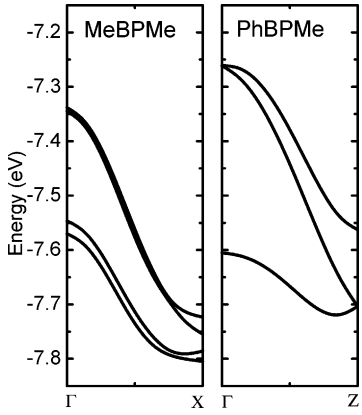

Figure 11. EHT dispersion curves for R_2BPMe **1** (R_2 = Me, Ph).

In the case of MeBPMe the four dispersion curves are grouped into two well-spaced pairs of crystal orbitals, indicative of an essentially 2-dimensional electronic structure. These features are readily interpreted in terms of the crystal packing (Figure 3), and the absence of intermolecular S−S interactions between the chains of radicals in the z direction. Lateral electronic communication along the y direction, however, remains substantial, although not as strong as that up and down the π-stacks. In PhBPMe the well-developed lateral interactions are demonstrated by the relatively wide separation of the three crystal orbitals. Indeed crystal orbital dispersion between the π-stacks is comparable to dispersion along the stacking direction. The total bandwidth W for the two compounds is on the order of 0.4−0.5 eV, which is comparable to the EHT bandwidths estimated for $ClBPR_1$[11] and $HBPR_1$[12] radicals, although less than is necessary to overcome the value of U for these systems.

Conclusions and Summary

The development of a simple, flexible 3-step procedure for producing the R_2BPR_1 **1** framework starting from a 4-substituted 2,6-dichloropyridine **3** opens the way for the design of new radical conductors. We have demonstrated the use of this technology in the preparation of two seminal examples, one with an alkyl and one with an aryl group in the R_2-position. The crystallographic results reveal how the relative sizes and shapes of the R_1 and R_2 substituents can dramatically affect the packing of radical π-stacks and hence the dimensionality of lattice-wide electronic interactions. When the two substituents (R_1 and R_2) are of similar size, the radical π-stacks pack into chain-like arrays. However, when one

(23) Bonner, J. C.; Fisher, M. E. *Phys. Rev. A* **1964**, *135*, 640.
(24) (a) Pal, S. K.; Itkis, M. E.; Reed, R. W.; Oakley, R. T.; Cordes, A. W.; Tham, F. S.; Siegrist, T.; Haddon, R. C. *J. Am. Chem. Soc.* **2004**, *126*, 1478. (b) Hicks, R. G.; Lemaire, M. T.; Ohrstrom, L.; Richardson, J. F.; Thompson, L. K.; Xu, Z. *J. Am. Chem. Soc.* **2001**, *123*, 7154.
(25) Britten, J. F.; Cordes, A. W.; Haddon, R. C.; Itkis, M. E.; Oakley, R. T.; Reed, R. W.; Robertson, C. M. *CrystEngComm* **2002**, *4*, 205.
(26) MeBPMe is monoclinic, and PhBPMe is trigonal. In neither case is there an exact equivalence of all the directions of the unit cell vectors in real and reciprocal space.
(27) (a) Whangbo, M.-H. *J. Chem. Phys.* **1979**, *70*, 4963. (b) Landrum G. A.; Dronkowski, R. *Angew. Chem., Int. Ed.* **2000**, *39*, 1560.

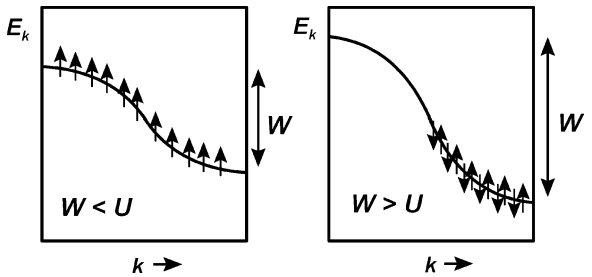

Figure 12. Schematic representation of the band filling for a neutral radical conductor with a Mott insulator (left) and metallic (right) ground state.

of the groups is more bulky, as in PhBPMe, clustering of the substituents, and therefore the radical π-stacks, can occur, to produce 2-dimensional networks of intermolecular S−S interactions. In the case of PhBPMe these tight (3.287(1) Å) S−S contacts are related by the 3-fold screw axes, and produce a unique close-packed array of molecular wheels.

Conductivity and magnetic measurements indicate that these materials are Mott insulators. Although substantial for a molecular species, the electronic bandwidth *W* arising from the interacting radicals is still insufficient to overcome the onsite Coulomb repulsion *U*; i.e., all levels of the conduction band are half-filled (Figure 12). However, the extremely close S−S interactions found in PhBPMe, and the concomitant observation of strong antiferromagnetic coupling, suggests the incipient formation of a chemical bond. Materials exhibiting larger bandwidths, a necessary condition for metallic ground state, cannot be far away.

Experimental Section

General Procedures and Starting Materials. The reagents ethyl cyanoacetate, ethyl benzoyl acetate, ethyl acetoacetate, phosphorus oxychloride, methyl trifluoromethanesulfonate (methyl triflate), ammonia gas, sulfur monochloride, and decamethylferrocene were obtained commercially and used as received. All solvents were of at least reagent grade; acetonitrile and dichloroethane were dried by distillation from P_2O_5. All reactions were performed under an atmosphere of dry nitrogen. 2,6-Dihydroxy-4-methylpyridine[28] and 2,6-dihydroxy-4-phenylpyridine[29] were prepared according to literature methods. Melting points are uncorrected. Infrared spectra (Nujol mulls, KBr optics) were recorded on a Nicolet Avatar FTIR spectrometer (at 2 cm^{-1} resolution) and visible spectra were collected using a Beckman DU 640 spectrophotometer. ^{1}H NMR spectra were run on a Bruker Avance 300 MHz NMR spectrometer. Elemental analyses were performed by MHW Laboratories (Phoenix, AZ).

Preparation of 2,6-Dichloro-4-methylpyridine 3 (R_2 = Me). 2,6-Dihydroxy-4-methylpyridine hydrochloride (12.5 g, 77.3 mmol) was added to 40 mL of $POCl_3$ (CAUTION: HCl gas evolution) in a Parr pressure reactor, which was heated to 180 °C for 5 h. The reactor was cooled to room temperature, and the contents were carefully added to 500 mL of crushed ice. The mixture was extracted 4× with ×200 mL of dichloromethane, and the extracts were combined, dried over K_2CO_3, and concentrated to dryness. The product **3** (R_2 = Me) was recrystallized from hexane; yield 11.3 g (68.5 mmol, 87%), mp 64−66 °C. IR: 3080 (w), 1585 (s), 1547 (s), 1246 (m), 1163 (s), 1101 (m), 986 (m), 911 (s), 845 (s), 808 (s), 538 (m) cm^{-1}. ^{1}H NMR (δ, $CDCl_3$): 7.07 (s, 2H), 2.32 (s, 3H). Anal. Calcd for $C_6H_5Cl_2N$: C, 44.48; H, 3.11; N, 8.65%. Found: C, 44.50; H, 3.19; N, 8.47%.

Preparation of 2,6-Dichloro-4-phenylpyridine 3 (R_2 = Ph). A mixture of 2,6-dihydroxy-4-phenylpyridine (8.37 g, 44.7 mmol) and 40 mL of $POCl_3$ was heated in a Parr pressure reactor to 145 °C for 16 h. The reactor was cooled to room temperature, and the contents were carefully added to 500 mL of crushed ice. The brown mixture was extracted 3× with ×150 mL of dichloromethane, and the combined extracts were dried over K_2CO_3 and concentrated to dryness. The product **3** (R_2 = Ph) was recrystallized from pentane; yield 4.89 g (21.8 mmol, 48%), mp 50−51 °C. IR: 1600 (w), 1580 (s), 1530 (s), 1496 (m), 1463 (m), 1417 (w), 1366 (s), 1316 (w), 1291 (w), 1234 (w), 1175 (s), 1120 (s), 1066 (w), 1000 (m), 985 (s), 869 (s), 810 (s), 767 (s), 695 (s), 628 (s) cm^{-1}. ^{1}H NMR (δ, $CDCl_3$): 7.47 (s, 2H), 7.58−7.61 and 7.49−7.51 (m, 5H).[30]

Preparation of *N*-Methyl-2,6-dichloro-4-methyl-pyridinium Triflate 4 (R_2 = Me). Methyl triflate (4.80 g, 29.2 mmol) was added to a stirred solution of 2,6-dichloro-4-methylpyridine **3** (R_2 = Me) (4.4 g, 27.1 mmol) in 30 mL of dichloroethane. After 30 min a heavy white precipitate began to form. The mixture was then cooled to −20 °C for 1 h, and the white precipitate was collected by filtration and washed with cold dichloroethane. The product **4** (R_2 = Me) was dried in vacuo and recrystallized from hot dichloroethane; yield 6.27 g (19.2 mmol, 71%), mp 137−138 °C. IR: 3075 (w), 3054 (w), 1616 (s), 1561 (w), 1549 (m), 1267 (s), 1237 (s), 1225 (s), 1180 (w), 1159 (s), 1144 (s), 1116 (m), 1082 (w), 1032 (s), 879 (w), 826 (w), 638 (s), 573 (w), 547 (w), 518 (w) cm^{-1}. ^{1}H NMR (δ, CD_3CN): 7.92 (s, 2H), 4.27 (s, 3H), 2.55 (s, 3H). Anal. Calcd for $C_8H_8Cl_2F_3NO_3S$: C, 29.46; H, 2.47; N, 4.29%. Found: C, 29.61; H, 2.29; N, 4.35%.

Preparation of *N*-Methyl-2,6-dichloro-4-phenyl-pyridinium Triflate 4 (R_2 = Ph). Methyl triflate (4.2 g, 25.7 mmol) was added to a stirred mixture of 2,6-dichloro-4-phenylpyridine **3** (R_2 = Ph) (4.89 g, 21.8 mmol) in 30 mL of dichloroethane. The reaction mixture was stirred for 16 h, and the white precipitate was collected by filtration, washed with cold dichloroethane, and dried in vacuo. The product **4** (R_2 = Ph) was recrystallized from hot dichloroethane; yield 5.91 g (15.2 mmol, 70%), mp 194−195 °C. IR: 3086 (w), 1613 (s), 1594 (m), 1540 (m), 1400 (m), 1260 (s), 1227 (s), 1152 (s), 1076 (w), 1035 (s), 890 (m), 833 (m), 777 (s), 690 (m), 641 (s), 573 (m), 516 (m) cm^{-1}. Anal. Calcd for $C_{13}H_{10}Cl_2F_3NO_3S$: C, 40.22; H, 2.60; N, 3.45%. Found: C, 40.39; H, 2.50; N, 3.45%. ^{1}H NMR (δ, CD_3CN): 8.38 (s, 2H), 7.94−7.96 and 7.64−7.70 (m, 5H), 4.35 (s, 3H).

Preparation of *N*-Methyl-2,6-diamino-4-methyl-pyridinium Triflate 2 (R_2 = Me). A solution of **4** (R_2 = Me) (16.5 g, 50.8 mmol) was cooled to 0 °C and saturated with ammonia gas. A white precipitate formed immediately and the solution became orange. The saturated solution was sealed in a glass pressure reactor and heated, with stirring, to 75 °C. After 16 h the vessel was cooled to room temperature and vented. The mixture was heated to reflux for an additional 2 h to release excess ammonia, cooled to room temperature, and the white precipitate was filtered off. The filtrate was concentrated to dryness and the product **2** (R_2 = Me) recrystallized from acetonitrile/dichloroethane (1:30) mixture; yield 13.2 g (45.9 mmol, 89%), mp 108−111 °C. IR: 3414 (m), 3349 (m), 3233 (m), 1672 (m), 1644 (m), 1499 (w), 1461 (s), 1275 (m), 1168 (m), 1025 (s), 818 (w), 639 (m), 516 (w) cm^{-1}. Anal. Calcd for $C_8H_{12}F_3N_3O_3S$: C, 33.45; H, 4.21; N, 14.63%. Found: C, 33.56; H, 4.14; N, 14.60%. ^{1}H NMR (δ, CD_3CN): 6.05 (s, 2H), 3.39 (s, 3H), 2.16 (s, 3H).

Preparation of *N*-Methyl-2,6-diamino-4-phenyl-pyridinium Triflate 2 (R_2 = Ph). A solution of **4** (R_2 = Ph) (4.29 g, 11.0 mmol) was cooled to 0 °C and saturated with ammonia

(28) (a) Cope, A. C.; Hofmann, C. M.; Wyckoff, C.; Hardenbergh, E. *J. Am. Chem. Soc.* **1941**, *63*, 3452. (b) Ames, D. E.; Bowman, R. E.; Grey, T. F. *J. Chem. Soc.* **1953**, 3008.

(29) (a) Balicki, R.; Kaczmarek, L.; Nanyka-Namirski, P. *Pol. J. Chem.* **1979**, *53*, 2491. (b) Kambe, S.; Saito, K.; Sakurai, A.; Hayashi, T. *Synthesis* **1977**, 841. (c) Al-Jallo, H. N.; Al-Biaty, A.; Al-Azawi, F. N. *J. Heterocycl. Chem.* **1977**, *14*, 1347.

(30) Mello, J. V.; Finney, N. S. *Org. Lett.* **2001**, *3*, 4263.

gas. A white precipitate formed immediately and the solution became yellow. The saturated solution was sealed in a glass pressure reactor and heated, with stirring, to 75 °C. After 16 h the vessel was cooled to room temperature and vented. The mixture was heated to reflux for an additional 2 h to release excess ammonia, cooled to room temperature, and the white precipitate was filtered off. The filtrate was concentrated to dryness and the product **2** (R_2 = Ph) recrystallized from acetonitrile; yield 3.03 g (8.64 mmol, 78%), dec > 250 °C. IR: 3421 (s), 3354 (s), 3249 (s), 1651 (s), 1587 (m), 1567 (s), 1491 (m), 1325 (w), 1252 (s), 1224 (s), 1194 (m), 1180 (s), 1153 (s), 1032 (s), 999 (w), 990 (w), 842 (w), 830 (m), 770 (s), 759 (w), 697 (m), 638 (s), 574 (m), 516 (m) cm^{-1}. Anal. Calcd for $C_{13}H_{14}F_3N_3O_3S$: C, 44.70; H, 4.04; N, 12.03%. Found: C, 44.94; H, 3.94; N, 11.86%. ^1H NMR (δ, CD_3CN): 7.64−7.50 (m, 5H), 6.49 (s, 2H), 6.11 (s, 4H), 3.46 (s, 3H).

Preparation of 8-Methyl-4-methyl-4*H*-bis[1,2,3]dithiazolo[4,5-b:5′,4′-e]pyridin-2-ium Trifluoromethanesulfonate [1][OTf] (R_1 = Me, R_2 = Me). Sulfur monochloride (1.50 mL, 2.53 g, 18.8 mmol) was added to a stirred solution of **2** (R_2 = Me) (2.00 g, 6.96 mmol) in 20 mL of a 1:1 acetonitrile/dichloroethane mixture. The initially green solution was heated at reflux for 5 h to afford a deep blue solution and red precipitate. The mixture was cooled to 0 °C and the product [**1**][OTf] (R_1 = Me, R_2 = Me) was filtered off, washed 3× with 50 mL of hot dichloroethane and dried in vacuo; yield 1.60 g (3.91 mmol, 56%). Recrystallization from hot acetonitrile afforded deep red plates, mp > 280 °C. IR: 1524 (w), 1409 (m), 1271 (s), 1247 (s), 1227 (s), 1162 (s), 1031 (s), 1012 (m), 934 (w), 861 (w), 738 (s), 722 (m), 681 (w), 670 (m), 639 (m), 516(w), 480 (m) cm^{-1}. Anal. Calcd for $C_8H_6F_3N_3O_3S_5$: C, 23.47; H, 1.48; N, 10.26%. Found: C, 23.20; H, 1.26; N, 10.00%. ^1H NMR (δ, CD_3CN): 3.59 (s, 3H), 2.34 (s, 3H).

Preparation of 8-Phenyl-4-methyl-4*H*-bis[1,2,3]dithiazolo[4,5-b:5′,4′-e]pyridin-2-ium Trifluoromethanesulfonate [1][OTf] (R_1 = Me, R_2 = Ph). Sulfur monochloride (3.00 mL, 5.06 g, 37.5 mmol) was added to a stirred solution of **2** (R_2 = Ph) (1.00 g, 2.86 mmol) in 20 mL of a 1:10 acetonitrile/dichloroethane mixture. The initially green solution was heated at gentle reflux for 16 h to afford a deep blue solution and a red precipitate. The mixture was cooled to 0 °C and the product [**1**][OTf] (R_1 = Me, R_2 = Ph) was filtered off, washed 3× with 50 mL of hot dichloroethane and dried in vacuo (1.17 g). Recrystallization from hot acetonitrile afforded lustrous red plates; yield 0.790 g, 1.67 mmol, 58%, mp > 280 °C. IR: 1529 (w), 1510 (w), 1414 (s), 1357 (s), 1249 (s), 1222 (s), 1207 (s), 1170 (s), 1057 (w), 1026 (s), 964 (w), 911 (w), 824 (w), 800 (s), 744 (s), 732 (s), 676 (s), 668 (s), 635 (s), 597 (w), 557 (m), 483 (s) cm^{-1}. Anal. Calcd for $C_{13}H_8F_3N_3O_3S_5$: C, 33.11; H, 1.71; N, 8.91%. Found: C, 33.31; H, 1.59; N, 8.70%. ^1H NMR (δ, CD_3CN): 7.73−7.55 (m, 5H), 3.65 (s, 3H).

Preparation of 8-Methyl-4-methyl-4H-bis[1,2,3]dithiazolo[4,5-b:5′,4′-e]pyridin-3-yl MeBPMe, 1 (R_1 = R_2 = Me). Decamethylferrocene (0.400 g, 1.22 mmol) was added to a solution of [**1**][OTf] (R_1 = R_2 = Me) (0.503 g, 1.22 mmol) in 12 mL of degassed (5 freeze−pump−thaw cycles) acetonitrile, and the resulting slurry was heated to reflux and stirred for 1 h. Green crystals of MeBPMe **1** (R_1 = R_2 = Me) were collected by filtration, washed 3× with 10 mL of acetonitrile, and dried in vacuo; yield 0.240 g, 0.92 mmol, 76%. The product was recrystallized from degassed (5 freeze−pump−thaw cycles) dichloroethane as metallic green needles. IR: 1503 (w), 1414 (w), 1241 (s), 1197 (w), 1001 (w), 915 (w), 821 (w), 716 (s), 689 (s), 656 (s), 637 (s), 510 (m), 510 (m), 485 (w), 465 (w) cm^{-1}. Anal. Calcd for $C_7H_6N_3S_4$: C, 32.29; H, 2.32; N, 16.14%. Found: C, 32.49; H, 2.10; N, 15.99%.

Preparation of 8-Phenyl-4-methyl-4H-bis[1,2,3]dithiazolo[4,5-b:5′,4′-e]pyridin-3-yl PhBPMe, 1 (R_1 = Me, R_2 = Ph). Decamethylferrocene (0.494 g, 1.51 mmol) was added to a solution of [**1**][OTf] (R_1 = Me, R_2 = Ph) (0.706 g, 1.50 mmol) in 15 mL of degassed (5 freeze−pump−thaw cycles) acetonitrile, and the resulting slurry was stirred for 1 h at room temperature. Red crystals of PhBPMe **1** (R_1 = Me, R_2 = Ph) were collected by filtration, washed 2× with 20 mL of acetonitrile and dried in vacuo; yield 0.448 g, 1.39 mmol, 93%. Recrystallization from hot, degassed (5 freeze−pump−thaw cycles) toluene afforded metallic red needles. IR: 1462 (s), 1377 (m), 1225 (m), 1184 (m), 1076 (w), 1043 (w), 973 (w), 954 (w), 915 (w), 886 (w), 796 (w), 780 (w), 733 (s), 692 (s), 663 (m), 655 (m) 551 (m), 463 (m) cm^{-1}. Anal. Calcd for $C_{12}H_8N_3S_4$: C, 44.69; H, 2.50; N, 13.03%. Found: C, 44.71; H, 2.68; N, 12.87%.

EPR Spectra. X-Band EPR spectra were recorded at ambient temperature using a Bruker EMX-200 spectrometer; samples of the radicals were dissolved in degassed dichloromethane. Hyperfine coupling constants were obtained by spectral simulation using Simfonia[31] and WinSim.

Cyclic Voltammetry. Cyclic voltammetry was performed using a PINE Bipotentiostat, model AFCClBP1, with scan rates of 50−100 mV s^{-1} on solutions (<10^{-3} M) of [**1**][OTf] (R_1 = Me, R_2 = Me, Ph) in CH_3CN (dried by distillation from P_2O_5 and CaH_2) containing 0.1 M tetra-*n*-butylammonium hexafluorophosphate as supporting electrolyte. Potentials were scanned with respect to the quasi-reference electrode in a single compartment cell fitted with Pt electrodes and referenced to the Fc/Fc^+ couple of ferrocene at 0.38 V vs SCE.[32] The $E_{pa}-E_{pc}$ separation of the reversible couples was within 10% of that of the Fc/Fc^+ couple.

X-ray Measurements. Crystals of MeBPMe **1** (R_1 = R_2 = Me) suitable for X-ray work were obtained by recrystallization from degassed dichloroethane. Crystals of PhBPMe **1** (R_1 = Me, R_2 = Ph) were grown by slow diffusion of a solution of Cp^*_2Fe in degassed acetonitrile into a solution of [**1**][OTf] (R_1 = Me, R_2 = Ph) in degassed acetonitrile. Samples for analysis were glued to a glass fiber with epoxy, centered on a Bruker P4/CCD diffractometer, and irradiated using 11.25 kW X-rays from a Bruker Mo rotating anode generator. Data sets on several crystals of MeBPMe **1** (R_1 = R_2 = Me) were collected using omega scans with a Bruker SMART6000 CCD detector on a D8 3-circle goniometer and parallel-focused Cu Kα radiation from a Rigaku RU-200 fine-focus rotating anode generator at 5 kW. The data were scanned using Bruker's SMART program and integrated using Bruker's SAINT software. For MeBPMe **1** (R_1 = R_2 = Me) the refinement reached a reasonable *R*-factor of 6.85%. High resolution data were limited by the fact that the data crystal was only a 5-μm-thick needle and it was twinned. There was no significant diffraction above 120°. The twinning was a result of a 180° rotation about the 2D Me−Me interface (the *ab* plane of the crystal). The twinning has no effect on the S−S intermolecular contacts or their direction.

Magnetic Susceptibility Measurements. Magnetic susceptibilities were measured over the temperature range 5−380 K on a George Associates Faraday balance operating at 0.5 T.

Band Calculations. Band electronic structure calculations were performed with the EHMACC suite of programs[33] using the Coulomb parameters of Baasch, Viste, and Gray[34] and a quasi-split valence basis set adapted from Clementi and Roetti;[35] numerical values are tabulated elsewhere.[36] The off-diagonal elements of the Hamiltonian matrix were calculated with the standard weighting formula.[37] Atomic positions were taken from the crystallographic data.

(31) WinEPR Simfonia, Bruker Instruments, Inc., Billerica, MA.
(32) Boeré, R. T.; Moock, K. H.; Parvez, M. *Z. Anorg. Allg. Chem.* **1994**, *620*, 1589.
(33) EHMACC, Quantum Chemistry Program Exchange, program number 571.
(34) Basch, H.; Viste, A.; Gray, H. B. *Theor. Chim. Acta* **1965**, *3*, 458.
(35) Clementi, E.; Roetti, C. *At. Data Nucl. Data Tables* **1974**, *14*, 177.
(36) Cordes, A. W.; Haddon, R. C.; Oakley, R. T.; Schneemeyer, L. F.; Waszczak, J. V.; Young, K. M.; Zimmerman, N. M. *J. Am. Chem. Soc.* **1991**, *113*, 582.
(37) Ammeter, J. H.; Bürgi, H. B.; Thibeault, J. C.; Hoffmann, R. *J. Am. Chem. Soc.* **1978**, *100*, 3686.

Acknowledgment. We thank the Natural Sciences and Engineering Research Council of Canada (NSERCC), the U.S. Office of Basic Energy Sciences, Department of Energy (Grant DE-FG02-97ER45668), and the Office of Naval Research (Contract No. N00014-99-1-0392) for financial support. We also thank the NSERCC for post-graduate scholarships to L.B. and O.P.C.

Supporting Information Available: Details of X-ray crystallographic data collection and structure refinement, tables of atomic coordinates, bond distances and angles, anisotropic thermal parameters, and hydrogen atom positions in CIF format. This information is available free of charge via the Internet at http://pubs.acs.org.

CM035191U